Rotational Changes Accompanying Vibrational Transfer in Low-Energy Collisions between Benzene and H_2, D_2, and CH_4†

Eric R. Waclawik and Warren D. Lawrance*

School of Chemistry, Physics and Earth Sciences, Flinders University, GPO Box 2100, Adelaide, South Australia 5001, Australia

Received: June 4, 2003; In Final Form: September 30, 2003

We have examined the changes in rotation that occur simultaneously with a change in vibrational state within a large polyatomic. Specifically, a variety of rotational-level population distributions have been prepared in the 6^1 vibrational level of $^1B_{2u}$ benzene, and the rotational distributions within 0^0 that result from collisions with H_2, D_2, or CH_4 have been observed by measuring the rotational contour of the 6_1^0 band in emission. The experiments were performed in the collision region of a supersonic free jet expansion at a translational temperature of 34 K (H_2 and D_2) or 18 K (CH_4). It is demonstrated that rotational-energy transfer within 6^1 and 0^0 does not obscure the rotational changes accompanying the vibrational change. For a particular collision partner, the final rotational distributions in 0^0 are essentially the same for all initial 6^1 distributions. However, the final 0^0 rotational distributions are quite different for the different collision partners. The observed 6_1^0 rotational contours are fit reasonably well by a thermal distribution with 0^0 rotational temperatures of 19, 41, and 93 K for H_2, D_2, and CH_4, respectively. The 6_1^0 rotational contours were also fit using an exponentially decaying momentum gap model to evolve the initial 6^1 rotational distribution to the final 0^0 distribution. As an illustration, for an initial *J*, *K* distribution with average *J* and *K* values of 8 and 6, respectively, the changes in these average values are (written as $(\Delta\bar{J}, \Delta\bar{K})$) (3, 1), (8, 4), and (16, 9) for the thermal distribution fits for H_2, D_2, and CH_4, respectively. The corresponding values for the momentum gap model are (4, 0), (10, 1), and (19, 8). The modeling shows that the $|\Delta K|$ changes are much larger for CH_4 than for H_2 and D_2. A possible reason for the relaxed ΔK restriction with CH_4 may be that a broad range of collision geometries leads to $6^1 \rightarrow 0^0$ vibrational-energy transfer with this partner. The 0^0 distributions for D_2 are broader than for H_2, illustrating that the reduced mass and rotational-level spacings play an important role in determining the rotational changes that occur.

I. Introduction

In 1975, Parmenter and Tang reported the first detailed state-to-state study of vibrational-energy transfer (VET) in a large polyatomic, monitoring transfer from the benzene 6^1 level (S_1, $^1B_{2u}$) with a variety of collision partners at room temperature.[1] This pioneering work established "propensity rules" for the preferred changes in the vibrational state induced by collisions and showed that the VET process can be highly efficient in polyatomics, being comparable to the elastic collision rate. A feature of the transfer was the similarity in state-to-state branching ratios among collision partners belonging to the same "class". Later room-temperature studies supported the conclusions reached by Parmenter and Tang.[2−4]

Recently, we reported an investigation of VET from 6^1 benzene caused by very low energy collisions with diatomic and small polyatomic molecules.[5] The branching ratios for the vibrational energy transferred from 6^1 to other vibrational levels were found to depend strongly on the collision partner. The influence of the collision partner was most evident for transfer to the ground vibrational level, 0^0. This transfer involves the smallest change in vibrational quanta (Δv) among the levels accessible from 6^1. It also involves the largest difference in energy (ΔE) between 6^1 and the S_1 vibrational states accessed during VET[1]. The 6^1-0^0 energy gap is 522 cm^{-1}.

To explain these observations, we proposed that the strong collision partner dependence for $6^1 \rightarrow 0^0$ transfer arises from angular momentum constraints in the collision. We argued that the angular momentum constraints were determined by (a) the mass and size of the collider, which governed the orbital angular momentum contribution to the interaction, and (b) the principal moments of inertia of the collision partner, which determined the amount of energy that could be partitioned into (internal) rotational angular momentum after the collision.

Further experimental evidence for the importance of angular momentum constraints in VET was obtained from analysis of the width of the observed rotational band contours of the 0^0 state and other VET destination states. Rotational band contour analysis revealed that the average value of the principal rotational quantum number *J* in the destination vibration also depended significantly upon the collision partner.[5] For instance, the average *J* values observed for polyatomic partners CH_4, C_2H_2, and *c*-C_3H_6 are ∼2 times greater than those observed for diatomic partners H_2, D_2, and N_2.

In this work, we investigate the issue of angular-momentum-mediated vibrational transfer using high-resolution time-resolved dispersed fluorescence (TRDF) techniques to observe in detail the rotational contours in collisionally populated states. The focus of the present study is the $6^1 \rightarrow 0^0$ transfer in S_1 benzene with collision partners H_2, D_2, and CH_4. We aim to determine the types of rotational changes that occur during VET and to explore the generality of trends by observing the 6_1^0 rotational

† Part of the special issue "Charles S. Parmenter Festschrift".

* To whom correspondence should be addressed. E-mail: warren.lawrance@flinders.edu.au. Fax: 61-8-8201 2905.

10.1021/jp035560+ CCC: $25.00
Published on Web 10/23/2003

contour with the three collision partners. Because of the small rotational constants for benzene, we prepare a narrow distribution of initial rotational states and measure the rotational contour for the terminal vibration. We are unable to identify individual initial and final *J, K, l* states.

McCaffery and co-workers have recently devised a simple model for the rotational changes that occur in diatomics during collisions,[6−8] van der Waals molecule dissociation[9] and elementary chemical reactions.[10] The model is based on the conversion of linear to angular momentum via a torque arm for the collision, operating within the energy constraints that apply. The model has been successfully applied to a number of diatomic systems.[6] It has recently been extended to include polyatomic systems.[11] The data obtained in our study will provide a useful test of this model. In this paper, we present the results of our experimental investigation and give an overview of the trends to emerge. The analysis of the results using McCaffery's model will be the subject of a future publication.

H_2, D_2 and CH_4 were chosen as the collision partners because they had been observed to induce transfer to widely different average *J* values in benzene in our previous low-resolution (5 cm^{-1}) study. H_2 and D_2 share the same intermolecular potential for interaction with benzene but have different reduced masses in the collision and different rotational-level spacings.

There are very few studies of rotational changes accompanying VET (i.e., rovibrational energy transfer). In small polyatomics, the rate of rotational relaxation is generally much larger than that for vibrational relaxation, and any initial disequilibrium produced in the initial rotational population is equilibrated within the starting vibrational level prior to VET.[3,12] For larger polyatomics, the presence of low-frequency modes can increase the cross section for VET, and it can become comparable to the RET cross section, allowing rovibrational energy transfer to be observed. Parmenter and co-workers' crossed molecular beam study of rovibrational energy transfer in glyoxal is perhaps the best example of rovibrational transfer in polyatomics, providing insight into the *K* changes that occur during VET in that molecule.[13]

II. Experimental Details

The experimental apparatus used to obtain TRDF spectra has been described in detail in a previous publication.[14] Briefly, collisions between benzene and the collision partner are monitored in the collision region of a supersonic expansion. As in our previous study,[5] the free jet expansion gas mixture consisted of ca. 1% benzene seeded in a carrier gas, which was either the collision partner (in the H_2 and D_2 cases) or a mixture of the collision partner and He (CH_4 case). TRDF spectra were recorded 4 mm downstream from a pulsed nozzle with a 0.8-mm diameter orifice (i.e., at X/D = 5). The frequency-doubled output of a pulsed dye laser (ca. 4-ns duration, 0.15-cm^{-1} fwhm for the fundamental) was tuned to chosen regions of the 6_0^1 band rotational contour (band origin υ_{00} = 38 606.089 cm^{-1} (vac)[15]) to prepare different *J, K, l* distributions in 6^1. The laser frequency was calibrated to the 6_0^1 band origin, υ_{00}, by fitting the 6_0^1 rotational contour measured by laser-induced fluorescence (LIF) to a calculated contour using the constants given in ref 15.

As previously, the 6^1 and 0^0 levels in benzene were monitored in dispersed fluorescence using the $6_0^1 1_1^0$ and 6_1^0 transitions, respectively. Emission was collected and dispersed using a 4.2-m home-built Czerny−Turner spectrometer and detected with a fast (2 ns) rise time photomultiplier tube (PMT). Dispersed fluorescence measurements were recorded in 0.3-cm^{-1} steps at 1-cm^{-1} spectral resolution. Low light levels at 1-cm^{-1} resolution required the use of single-photon counting techniques.

Fluorescence signals detected by the PMT were stored in a 250-MHz digitizing oscilloscope operated with a sampling rate of 10^9 samples s^{-1} (HP54510A). The oscilloscope recording for each laser shot was transferred to a computer and subsequently processed to obtain the delay time of each photon peak. The time axis was segmented into bins of 10-ns width, and the photon count within a particular bin was incremented when the delay time fell within its 10-ns interval. Data were recorded to 500 ns after the laser pulse, 5−6 times the fluorescence lifetimes of the 0^0 and 6^1 states of 106 and 87 ns, respectively.[16−18] A histogram of photon count versus delay time was produced at each wavelength setting of the spectrometer, producing data in the form of a 3D surface in which the fluorescence intensity was recorded as a function of both wavelength and time. Typically, recordings were made for 300 laser shots at each spectrometer grating position to obtain adequate signal-to-noise levels.

For H_2 and D_2, the free jet expansion translational temperature was calculated to be 34 K at X/D = 5. This was confirmed by fitting calculated contours to laser-induced fluorescence (LIF) spectra of the 6_0^1 rotational band contour, with temperature as the variable. For methane, measurements were taken using a mixture of 20% CH_4 in He at 60 kPa backing pressure. This low backing pressure (0.6 atm) precludes significant van der Waals complex formation. Helium has previously been shown to be an inefficient relaxer of 6^1 benzene under similar conditions.[14,19−22] In particular, state-to-state data shows the relaxation of 6^1 by He to populate 11^1, 16^1, and 16^2, with no population of 0^0 observed. Thus, the possibility of a contribution to $6^1 \rightarrow 0^0$ transfer from He could safely be ignored. The rotational band contour of the 6_0^1 transition was also measured for the CH_4/He expansion and was found to be well fit by a single temperature of 18 K, equal to the translational temperature obtained from calculations using heat capacity ratios.[23]

III. Results

The results are presented as follows. Initially, we provide background spectroscopic information for benzene relevant to understanding the subsequent discussion of the rotational states populated. This is followed by a description of the initial 6^1 rotational distributions and a discussion of the comparison between the dispersed fluorescence spectra predicted from these distributions and those observed. We then present the results of experiments investigating the extent to which rotational energy transfer (RET) within either the initial state, 6^1, or final state, 0^0, might confound the measurement of rotational changes accompanying VET. Finally, for each of the collision partners we present the rotational contours for 0^0 arising from VET from a selected set of rotational states in 6^1.

A. Spectroscopy of Benzene. The S_1-S_0 transition in benzene has been extensively studied, and its spectroscopy is well understood.[24−26] The rotational selection rules for a perpendicular electronic transition in an oblate symmetric top require $\Delta J = 0, \pm 1$ and $\Delta K = \pm 1$.[27] The values of the benzene constants are known to high accuracy following the elegant work of Riedle et al.,[15] Callomon et al.,[28] and others.[29,32] Expressions for the rotational components of the 6_0^1, $6_0^1 1_1^0$, and 6_1^0 transitions are also given in these publications. (6_0^1 is used to prepare the initial 6^1 population, and $6_0^1 1_1^0$ and 6_1^0 are used to probe the 6^1 and 0^0 populations, respectively.) The relevant constants are listed in Table 1.

TABLE 1: Benzene S_0 and S_1 Rotational Constants Used to Simulate Rotational Band Contours[a]

molecule	state	B/cm^{-1}	C/cm^{-1}	ξ^{eff}
benzene	S_0	0.189762	$C = B/2$	−0.6
	6^1	0.181778	0.090865	−0.6
hydrogen	$^1\Sigma_g^+$	60.809[b]		
deuterium	$^1\Sigma_g^+$	30.429[b]		
methane	A, F, E[c]	5.241[d]		

[a] Rotational constants are taken from refs 15, 28, and 29. The ground-state rotational constants of the three collision partners used in this study are shown for comparison (refs 27 and 30). [b] Reference 27. [c] Only the lowest rotational levels of these CH_4 nuclear spin manifolds are likely to be populated in the free jet expansion. See ref 31 for a concise description of CH_4 spectroscopy and collisional selection rules. [d] Reference 30.

6_0^1 in absorption and 6_1^0 in emission each involve a transition from a nondegenerate to a degenerate vibrational state. For degenerate vibrations, there is a Coriolis coupling of the vibrational and rotational angular momenta. Rotational selection rules for Coriolis coupled states require that $\Delta K = +1$ transfer leads to $+l$ states and $\Delta K = -1$ transfer leads to $-l$ states in absorption, whereas in emission $\Delta K = +1$ transfer leads to $-l$ states and $\Delta K = -1$ transfer leads to $+l$ states.[32]

B. Determination of the 6^1 *J, K, l* Population Distribution: Initial States Populated. To establish the rotational changes accompanying $6^1 \rightarrow 0^0$ VET, we need to know the initial population distribution for the 6^1 *J, K, l* rotational levels. Many benzene rotational lines overlap within the pulsed dye laser bandwidth (ca. 0.3 cm^{-1}), and depending upon the exact offset of the laser pump frequency from the 6_0^1 absorption band center at $\upsilon_{00} = 38\,606.089$ cm^{-1},[15] markedly different *J, K, l* distributions can be formed. These distributions can be calculated as discussed below. The calculations can be checked by comparing the $6_0^1 1_1^0$ rotational contours observed in dispersed fluorescence with those predicted.

We noted earlier (section II) that the ground-state *J, K, l* distributions of benzene seeded in free jet expansions containing H_2, D_2, and CH_4 are adequately described by a single temperature. The rotational-level population distributions produced in 6^1 were predicted for each laser position by the following procedure:

(1) The Maxwell−Boltzmann distribution of S_0 benzene *J, K, l* states was calculated appropriate to the free jet expansion conditions (34 K for H_2 and D_2; 18 K for CH_4/He).

(2) The intensities of 6_0^1 rotational transitions within ±1 cm^{-1} of the center frequency of the dye laser were calculated and convoluted with a 0.3-cm^{-1} fwhm Gaussian function accounting for the (frequency-doubled) laser line width to give the relative populations for the rotational states within 6^1 excited by the laser. Those rotational states in 6^1 with populations of $<0.01\%$ of the most populated rotational level were ignored when subsequently calculating fluorescence emission.

(3) The calculated 6^1 distribution was used to compute the rotational profile of the $6_0^1 1_1^0$ band in emission for comparison with experimental contours. The intensities of the $6_0^1 1_1^0$ fluorescence transitions were convoluted with a 1-cm^{-1} fwhm Gaussian function that represented the slit function (i.e., resolution) of the spectrometer.

The laser frequency offsets from 6_0^1 υ_{00} are given in Table 2. The laser-induced population distribution within 6^1 for each of these offsets is succinctly described through the mean ($\bar{J}$ and $\bar{K}$) and root-mean-square deviation (J_{rms} and K_{rms}) for the rotational quantum numbers associated with the distribution.

TABLE 2: Positions within the 6_0^1 Rotational Contour Used to Excite Different Initial *J, K* Distributions within the 6^1 Level of Benzene[a]

separation from υ_{00}/cm^{-1}	collision partner	$\bar{J} \pm J_{rms}$	$\bar{K} \pm K_{rms}$[b]
3.05	H_2	7.6 ± 0.5	6.0 ± 2
	CH_4	12.3 ± 0.7	9.5 ± 3.1
1.2	H_2, CH_4	4.0[c]	3.4 ± 0.7
−0.2	H_2, D_2	7.6 ± 3.0	3.4 ± 2.9
	CH_4	6.5 ± 2.4	2.4 ± 3.8
−3.1	H_2, D_2, CH_4	7.7 ± 0.4	6.1 ± 1.9
−4.7	H_2, D_2	11.4 ± 0.8	8.6 ± 3.0
	CH_4	11.4 ± 0.7	8.8 ± 3.0
−6.4	H_2	14.9 ± 1.0	10.9 ± 3.9
	CH_4	15.0 ± 1.0	11.5 ± 3.8

[a] Laser frequencies are given in terms of their offset from $\upsilon_{00} = 38\,606.089$ cm^{-1}. For each laser position, the average *J* and *K* values excited, $\bar{J}$ and $\bar{K}$, and their root-mean-square deviations, J_{rms} and K_{rms}, are also given. [b] $\bar{K}$ and K_{rms} refer to $|K|$. [c] $J = 4$ is essentially the only *J* value populated.

These values are included in Table 2. A feature of the distributions is that, with the exception of the $\upsilon_{00} - 0.2$ cm^{-1} distribution that is in the Q-branch region, they are generally quite narrow in *J* but broader in *K*. We note that the value of $\bar{J}$ varies from 4 to 15, depending on the positioning of the laser within the rotational contour. There is thus a reasonably broad range of initial $\bar{J}$ values given by the various laser positions. We also note that, although the CH_4/He expansion is colder than the diatomic expansions, because of the shape of the 6_0^1 rotational contour, for most of the laser positions the distributions are very similar.

Comparisons of the calculated $6_0^1 1_1^0$ fluorescence spectra with the observed spectra at different laser positions within the 6_0^1 rotational contour reveal excellent agreement. The significant changes in the shape of the contour associated with different laser positions are well reproduced. This shows that the relative populations of the 6^1 rotational levels produced by laser excitation are accurately predicted.

C. Rotational-Energy Transfer Within 6^1. The experiment aims to measure the transfer of population from a narrow distribution of rotational levels in 6^1 to a distribution of rotational levels in 0^0. Rotational relaxation occurring within either 6^1 or 0^0 has the potential to erase the effect we seek. Consequently, the extent of rotational relaxation occurring within the initial and final vibrational levels needs to be assessed. Because the rate of rotational relaxation is generally not sensitive to the identity of the vibrational level involved,[13,33,34] rotational relaxation will occur within 6^1 and 0^0 at similar rates. Thus, we need to establish the extent to which rotational relaxation occurs in either state in order to assess the extent to which this may be a problem. This is done most straightforwardly in 6^1 because we initially prepare a nonequilibrium distribution within this state.

In the ground electronic state of a diatomic or small polyatomic molecule, the time scales for inelastic collisions are generally such that the lifetimes, τ, for rotational energy transfer (RET) and VET are $\tau_{RET} \ll \tau_{VET}$ (i.e., RET is generally significantly more efficient than VET[12]). However, in larger polyatomics such as benzene, the cross sections for vibrational relaxation are comparable to, and often exceed, hard sphere values,[3] and rotational relaxation cross sections are of only slightly higher magnitude.[33,34] On the basis of the room-temperature values, τ_{RET} is expected to be only a factor of ~2 less than τ_{VET}. One of the few systematic studies of state-to-state transfer in a large polyatomic that explores this issue is

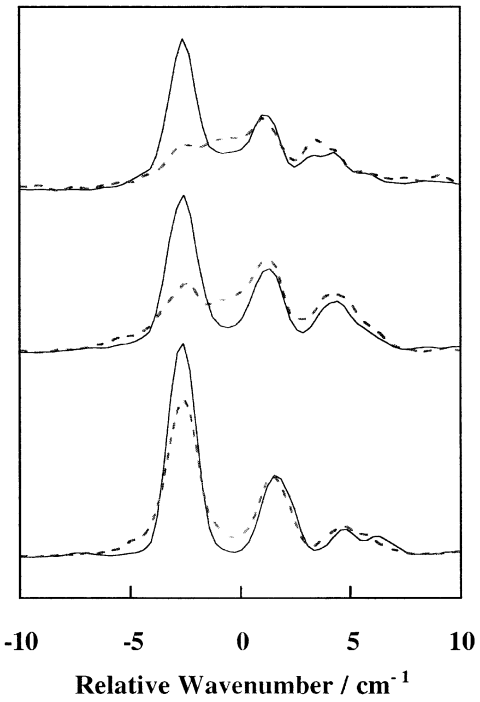

Figure 1. $6_0^1 1_1^0$ rotational contours at short (0−50 ns; —) and long (150−200 ns; − − −) delay times following the excitation of 6^1 for H_2 (upper trace), D_2 (middle trace), and CH_4 (lower trace) as the collision partners. The contours shown are for excitation at $\upsilon_{00} - 4.7$ cm^{-1}. A change in the contours between short and long times indicates rotational relaxation occurring within 6^1.

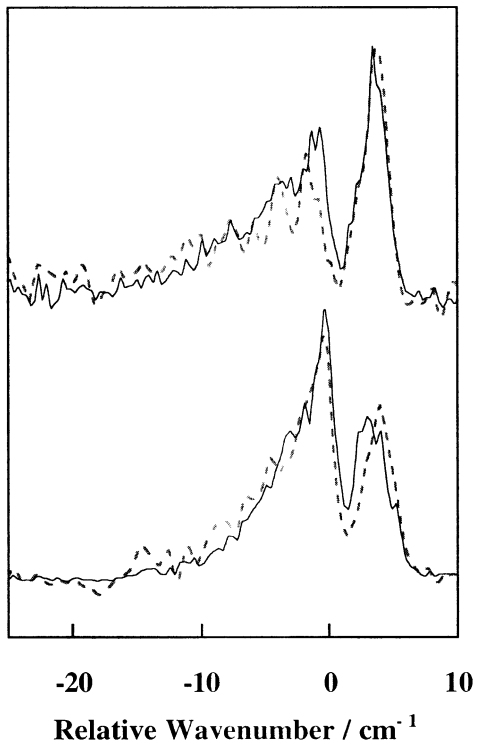

Figure 2. Comparison between the 6_1^0 rotational contour at short delay times (0−50 ns; − − −) and the time-integrated (0−400 ns; —) contour for H_2 (upper trace) and D_2 (lower trace) as the collision partners. Excitation of 6_0^1 is at $\upsilon_{00} - 3.1$ cm^{-1}. The similarity between the short and integrated contours indicates that rotational relaxation in 0^0 and 6^1 does not affect the 0^0 distribution significantly.

the study of S_1 glyoxal by Parmenter and co-workers. They observed that the cross sections for rotational transfer are of the same order of magnitude as those for rovibrational transfer.[13,35,36]

Rotational relaxation within 6^1 could be readily detected through a comparison of the dispersed fluorescence $6_0^1 1_1^0$ rotational contours at different delay times after the excitation pulse. RET appears through a change in the rotational contour with time as the initial distribution is redistributed through collisions. Figure 1 shows $6_0^1 1_1^0$ rotational band contours at short (0−50 ns) and long (150−200 ns) delay times for CH_4, D_2, and H_2. Less than one fluorescence lifetime is represented by 0−50 ns, and 150−200 ns represents ca. two fluorescence lifetimes.

For CH_4, the spectra show that there is little rotational relaxation, even at large delay times, so there will be negligible distortion of the nascent rotational distribution in 6^1 and 0^0 for CH_4/He free jet expansions.

For H_2 and D_2, higher backing pressures are required to observe $6^1 \rightarrow 0^0$ transfer. Figure 1 reveals rotational relaxation from the initial 6^1 rotational distribution, particularly for H_2. This suggests that the VET cross section is decreased compared to the RET cross section for H_2 and D_2. For H_2, we find that the rotational contours for different initial distributions become increasingly similar at longer time. Importantly, however, whereas RET is clearly evident, the rotational population remains far from thermal. The issue to be addressed for H_2 and D_2 is whether the RET observed is sufficient to obscure the angular momentum changes accompanying VET. To explore this issue, we examine the time-resolved rotational contours for the collisionally populated 0^0 level.

D. Rotational-Energy Transfer Within 0^0. Our aim is to measure the time-integrated 6_1^0 rotational contours to determine the rotational distribution produced within 0^0. A key issue is the extent to which these contours are influenced by rotational relaxation.

At early times, there is little opportunity for RET scrambling of the initial 6^1 distribution or of the resulting 0^0 distribution. By comparing the early-time 0^0 distribution with the time-integrated distribution, we are able to assess whether RET is affecting the results. Comparisons between the time-integrated 6_1^0 rotational band contours and those at short delay times are shown in Figure 2 for free jet expansions of H_2 and D_2. Because the 0^0 population has a rise time corresponding to the 6^1 decay time (∼87 ns), there is little population in 0^0 in the 0−50-ns interval. The time-integrated spectrum thus has only a minor contribution from the 0−50-ns interval. The low signal levels in the 0−50-ns spectra need to be allowed for when comparing the early-time and time-integrated spectra.

The 0−50-ns and time-integrated contours are quite similar and distinctly different from the contours associated with emission from 6^1. The data suggest that rotational relaxation does not significantly shift the nascent 0^0-level rotational distributions arising from VET for our experimental conditions. Rotational relaxation in 0^0 with CH_4/He expansions was examined and found to be negligible. The similarity between the time-integrated and 0−50-ns 0^0 contours reveals that rotational relaxation occurring in 6^1 prior to VET has little impact on the rotational distribution observed in 0^0.

E. 6_1^0 Rotational-Band Contours. High-resolution 6_1^0 TRDF spectra were recorded for the laser energies and corresponding *J, K, l* distributions listed in Table 2. We have shown in sections C and D that rotational relaxation has little influence on the 6_1^0 rotational-band contours. Comparing the 6_1^0 contours for different initial distributions should reveal whether the 0^0-level *J*,

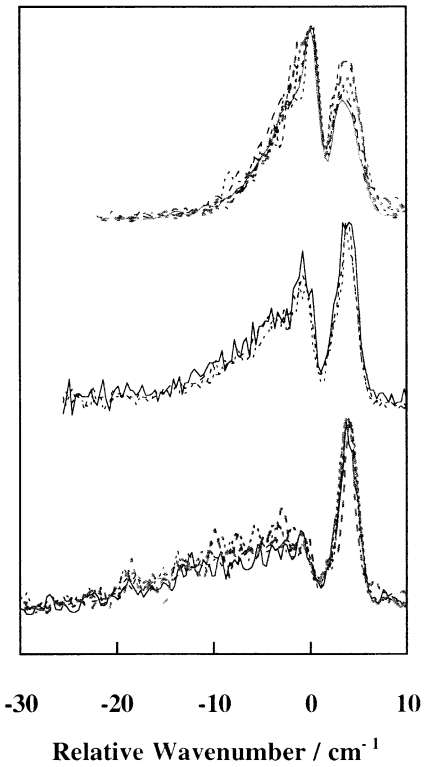

Figure 3. 6_1^0 rotational contours following excitation of the six initial rotational distributions within 6^1 for H_2 as the collision partner (upper trace), the three initial rotational distributions within 6^1 for D_2 as the collision partner (middle trace), and the six initial rotational distributions within 6^1 for CH_4 as the collision partner (lower trace). The excitation positions are given in Table 2. Note (i) the similarity in the contours for a particular collision partner, indicating that the final 0^0 distribution is not sensitive to the initial 6^1 distribution, and (ii) the differences between contours for different collision partners.

K, *l* distribution is dependent upon the initial 6^1 rotational distribution. In Figure 3, the 6_1^0 rotational band contours are compared at different laser positions for H_2, D_2, and CH_4. The Figure shows that for a particular collision partner the contours are very similar, showing little variation with the initial 6^1 distribution. It also shows that the contours are different for each collider. The rotational changes accompanying the $6^1 \rightarrow 0^0$ vibrational change therefore appear to be rather insensitive to the 6^1 *J*, *K*, *l* distribution but are quite sensitive to the collision partner. Because the interaction occurs on the same potential energy surface for H_2 and D_2, the differences must be associated with the increased mass for D_2. Parmenter and co-workers have shown through crossed molecular beam studies of rovibrational energy transfer in S_1 glyoxal that the reduced mass can play a dominant role in determining the relative rovibrational transfer cross sections.[13]

In our earlier 5-cm^{-1}-resolution study of VET from the 6^1 level of benzene, we found that the rotational band contour of the 6_1^0 transition could be replicated using a simple Maxwell−Boltzmann distribution for a variety of collision partners, including the three examined here.[5] Consequently, we have fitted the observed contours to thermal distributions with the upper 0^0 rotational energy constrained to <522 cm^{-1} to avoid exoergic transfer. The fits are shown in Figure 4. Given the similarity between rotational contours for each initial 6^1 distribution, for the purpose of this comparison we have added them together to give an average contour for each collision partner. It appears that the rotational contours calculated for thermal distributions match the observed contours quite well. The best-fit 0^0 rotational

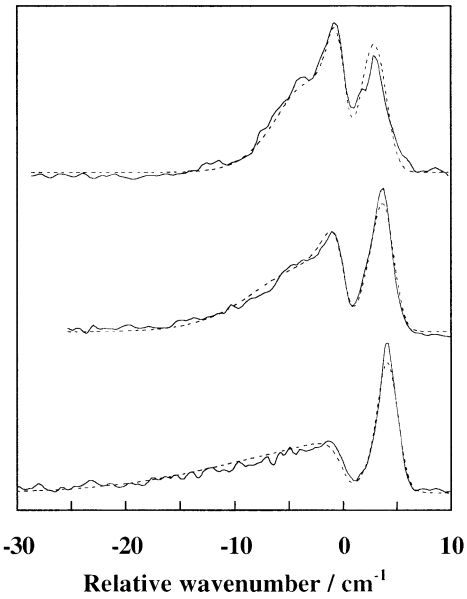

Figure 4. Thermal fits to the averaged 6_1^0 rotational contours for the three collision partners. The 0^0 rotational temperatures of best fit are 19, 41, and 93 K for H_2, D_2, and CH_4, respectively.

temperatures are 19, 41, and 93 K for H_2, D_2, and CH_4, respectively. The average *J* values, $\bar{J}$, for these distributions are 10.5, 15.7, and 23.8, respectively. The H_2 temperature is well below the translational temperature of the expansion (34 K), and the CH_4 temperature is well above the expansion temperature of 18 K. This shows that the 0^0 "rotational temperature" is not a consequence of the rotational distribution being in equilibrium with the translational temperature. The increase in rotational temperature from H_2 to D_2 to CH_4 is consistent with our previous low-resolution measurements and can be rationalized in terms of the angular momentum changes required.[5]

The temperatures from the high-resolution fits of 19, 41, and 93 K for H_2, D_2, and CH_4, respectively, compare with values of 29, 37, and 225 K extracted from the earlier 5-cm^{-1}-resolution data. Given the lower resolution of this earlier data, the H_2 and D_2 values agree surprisingly well with the new higher-resolution data. The earlier CH_4 temperature is significantly higher than the temperature that has been determined here. This arises as follows. The characteristic feature of the benzene rotational contour is a sharp edge on the high-wavenumber side, where the ^{P}R and ^{R}R branch's fortrat parabolas reverse direction.[28] The disposition of the various R branches results in a sharp intensity maximum that is very sensitive to the rotational-level populations. When fitting the low-resolution data, differences in the R branch-head intensity from the predicted thermal distribution can lead to the fitted temperatures having large uncertainties. The thermal fit to the high-resolution contour underestimates the R-branch intensity.

IV. Discussion

A number of features of the rotational changes accompanying $6^1 \rightarrow 0^0$ VET are apparent from the data and its preliminary analysis presented above. First, the final 0^0 rotational distribution has surprisingly little dependence on the initial 6^1 distribution. Second, it follows that the almost constant $\bar{J}$ value for the final distributions requires quite different values of $\Delta\bar{J}$ given the span of $\bar{J}$ values in the initial distributions. For example, for H_2 the initial values of $\bar{J}$ span the range of 4−15, and the final $\bar{J}$ estimated from the thermal fit to the distribution is ∼10. This leads to $\Delta\bar{J}$ in the range of −5 to 6. For CH_4, $\bar{J}_{initial}$ also spans

TABLE 3: Values of Parameters α and β Used to Describe the Changes in J and K Associated with Vibrational Transfer $6^1 \rightarrow 0^0$ [a,b]

laser energy offset from 6_0^1 υ_{00}/cm^{-1}	H_2		D_2		CH_4	
	α	β	α	β	α	β
−0.2	0.16	0.1	0.1	0.1	0.1	0.001
−3.1	0.25	1	0.14	0.1	0.1	0.001
−4.7	[c]	[c]	0.15	0.1	0.1	0.001

[a] See eq 1. [b] The parameters shown are those that provide the best fit to the experimental 6_1^0 rotational contours. The initial distributions are determined by the different laser positions within the 6_0^1 rotational contour. [c] The momentum gap model could not provide an acceptable fit.

the range of 4−15, and $\bar{J}_{\text{final}}$ is ∼23, giving $\Delta\bar{J}$ values of ∼8−19. Third, the average angular momentum within the VET destination state increases with increasing collision partner mass.

Although modeling the rotational distributions in 0^0 using a Boltzmann distribution gives reasonable fits to the observed contours, such an analysis does not provide insights into the rovibrational transfer. To try to gain such insights, we investigated a simple angular momentum model for the rotational changes that occur during VET. There is mounting evidence that angular momentum changes control such transfer.[6−8,37] Our previous work on benzene concluded that angular momentum constraints play a substantial role in determining the state-to-state vibrational preferences seen in benzene VET.[5] Our model assumes exponential dependencies for the probability of ΔJ and ΔK changes during the transfer, leading to the simple relation

$$P \propto (2J_f + 1)e^{-\alpha|J_f - J_i|}\, e^{-\beta|K_f - K_i|} \qquad (1)$$

The preexponential factor $(2J_f + 1)$ takes into account the benzene rotational-state degeneracy in the VET destination state. The probability of endoergic transfer was assumed to be insignificant at the collision energy conditions of the free jet expansion, and P was set equal to 0 when $E_f^{\text{rot}} > E_i^{\text{rot}} + \Delta E_{\text{vib}}$. Symmetry restrictions on transfer are ignored in this model. Nevertheless, a qualitative appreciation of trends in ΔJ and ΔK may be identified.

To fit the observed rotational contours, the values of α and β were varied to obtain 0^0 rotational distributions from which simulated 6_1^0 rotational band contours were produced for comparison with the observed contours. The best matches to experiment provide an estimate of the ΔJ and ΔK changes that occur with each collision partner at each excitation laser energy. The best fits were determined by minimizing the residuals between the experimental and simulated contours. The best-fit values of α and β are presented in Table 3 for each collision partner at the three laser offsets of −0.2, −3.1, and −4.7 cm^{-1}. These are the only positions for which we have data for all three partners. The parameters required to fit the data depend on the initial rotational distribution, particularly for H_2 where an acceptable fit could not be obtained using this model for a laser offset of −4.7 cm^{-1}. Representative fits to the data for the laser position of υ_{00} − 0.2 cm^{-1} are presented in Figure 5. We find that the fits are qualitatively similar to those obtained for a Boltzmann distribution within the final state. Note, however, that the contours do not sufficiently resolve the rotational structure for the values of α and β to be other than indicative.

The final J, K distributions obtained from the model differ in detail from the thermal distributions but generally have a similar overall shape. This is illustrated in Figure 6, where the model distributions are compared with the thermal distributions.

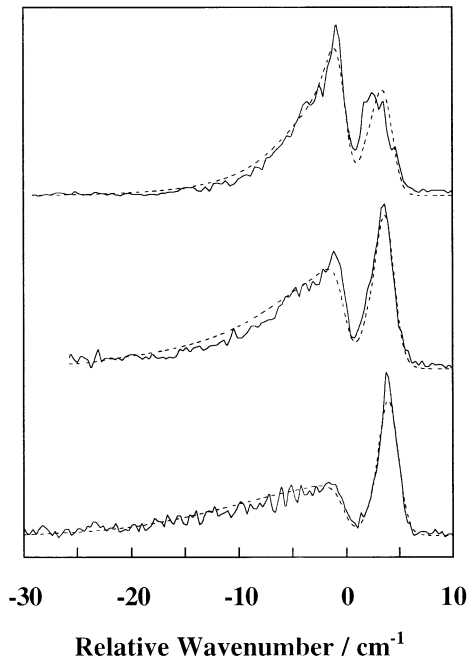

Figure 5. Fits of eq 1 to the averaged 6_1^0 rotational contours for H_2, D_2, and CH_4. The fits shown are for the initial 6^1 distribution produced by excitation at υ_{00} − 0.2 cm^{-1}.

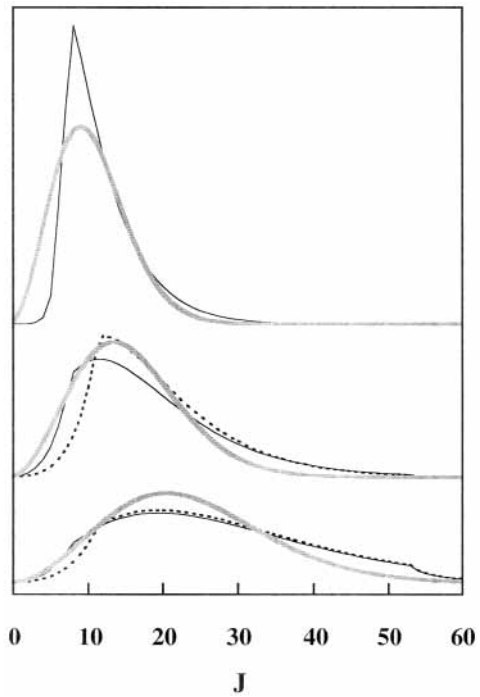

Figure 6. Thermal and model (eq 1) distributions that provide the best fits to the averaged 6_1^0 rotational contours for H_2 (upper traces), D_2 (middle traces), and CH_4 (lower traces). The J distributions are obtained by summing all of the K-state populations for a particular J. For clarity, the model fits are shown for only two laser positions, υ_{00} − 3.1 cm^{-1} (—) and υ_{00} − 4.7 cm^{-1} (− − −). Note that for H_2 the model does not give an acceptable fit for υ_{00} − 4.7 cm^{-1}. The thermal distributions are shown as gray lines. The average J and K values, $\bar{J}$ and $\bar{K}$, and the root-mean-square deviations, J_{rms} and K_{rms}, for these distributions are given in Table 4.

This Figure compares the J distributions by summing all of the K-state populations for a particular J. The plot clearly shows the final state distributions moving to higher J values and broadening across the series H_2, D_2, CH_4. The momentum gap model distributions for D_2 and CH_4 do not drop as rapidly at

TABLE 4: Average *J* and *K* Values, $\bar{J}$ and $\bar{K}$, for 0^0 as Determined from the Model and Thermal Distributions for the Distributions Shown in Figure 6[a]

collision partner	6_0^1 laser offset[b]/cm^{-1}	type of fit	$\bar{J} \pm J_{rms}$	$\bar{K} \pm K_{rms}$
H_2	−3.1	model	11.9 ± 5.1	6.0 ± 1.3
		thermal	10.5 ± 4.8	6.8 ± 5.1
D_2	−3.1	model	18.2 ± 9.5	7.1 ± 5.5
	−4.7	model	19.4 ± 8.8	8.3 ± 5.7
		thermal	15.7 ± 7.1	9.9 ± 7.5
CH_4	−3.1	model	26.8 ± 13.0	14.0 ± 11.6
	−4.7	model	27.6 ± 12.6	14.4 ± 11.6
		thermal	23.8 ± 10.6	15.0 ± 11.3

[a] Also shown are the root-mean-square deviations, J_{rms}, K_{rms}. [b] For H_2, the model does not provide an acceptable fit for a laser offset of −4.7 cm^{-1}.

high *J* as do the thermal distributions, and this results in their having slightly higher average *J* values. For H_2 and D_2, the thermal distributions are broader in *K* than those of the model; however, the model distribution is slightly broader than the thermal distribution for CH_4. Table 4 shows the average *J* and *K* values, $\bar{J}$ and $\bar{K}$, for 0^0 as determined from the model and thermal distributions shown in Figure 6. The root-mean-square deviations, J_{rms}, K_{rms}, are also shown. The differences in these distributions, which give fits to the observed contours of comparable quality, illustrate the level of uncertainty involved in determining *J*, *K* distributions from the observed contours.

The essential feature of the model is that small α and β values in eq 1 predict that large ΔJ and ΔK changes will occur during the transfer. The converse is true for large values of α and β. Comparing the fitted parameters in Table 3 for the different collision partners, we can see that for hydrogen the average ΔJ and ΔK changes are comparatively small. For laser pumping at −0.2 cm^{-1}, a much larger range of 6^1 *J*, *K* levels was populated than for the other laser positions. Nevertheless, the values of α and β (and thus the average ΔJ and ΔK changes during the collision) were observed to be similar.

Comparing H_2 with D_2, we see that the values of α and β are slightly smaller for D_2. The laser-prepared 6^1 rotational population distributions are the same for D_2 and H_2 because the free jet temperatures are the same. That slightly larger α and β parameters are needed for the best-fitting simulated spectra implies that slightly larger angular momentum changes occur in both *J* and *K* of benzene for collisions with D_2.

When methane is the collision partner, α is 0.1, compared with 0.1−0.15 for D_2 and 0.16−2.5 for H_2. This suggests that the ΔJ changes that occur during the VET process for CH_4 are somewhat larger than those for D_2 and considerably larger than those for H_2. In contrast, the fitted parameter β for methane is 0.001, considerably smaller than the β parameters obtained from fits to the D_2 and H_2 data. It thus appears that large changes in *K* are much more probable for CH_4 than for H_2 or D_2. We note that this is not an artifact of there being significantly different initial rotational populations in 6^1 arising from the different temperatures of the expansions. We pointed out in section IIIB that the 6^1 rotational population distributions are very similar for the diatomic and CH_4/He expansions.

From the initial and final $\bar{J}$ and $\bar{K}$ values given in Tables 2 and 4, the changes in the average values of *J* and *K* can be determined. By way of illustration, for $\upsilon_{00} - 3.1$ cm^{-1} the changes are (written as ($\Delta\bar{J}$, $\Delta\bar{K}$)) (3, 1), (8, 4) and (16, 9) for the thermal distribution fits for H_2, D_2, and CH_4, respectively. The corresponding values for the momentum gap model are (4, 0), (10, 1), and (19,8).

With the much smaller value of β for CH_4, the momentum gap model suggests that there are much larger $|\Delta K|$ changes associated with this species compared with those for H_2 and D_2. The large value of $|\Delta K|$ implies that for a given (small) ΔJ change in benzene all allowed 0^0 *K* states may be populated with equal probability during the interaction with CH_4. Because *K* is the projection of *J* onto the unique rotational axis, the enhanced range of *K* states accessed for CH_4 may indicate that a wider range of approach geometries cause the deactivation of the in-plane 6^1 vibration.

Why do the results here show a similar trend to pure rotational transfer (an exponential falloff in probability with ΔJ)? Studies of rovibrational transfer in polyatomic molecules have often concentrated on simultaneous vibrational and rotational excitation using crossed-beam and UV-pump/IR-probe techniques.[13,35,36,38] The rotational-transfer probability typically increases from $\Delta J = 0$ to a maximum ΔJ_{peak} before the onset of an exponential-like falloff. This type of behavior has been explained by considering the influence of restrictions on ΔJ probabilities by McCaffery.[6−8,39] The analysis predicts a peak in the ΔJ distribution because vibrational excitation requires collisions to overcome a threshold energy (or linear angular momentum) before angular momentum changes can take place. Interconversion of linear and angular momenta is constrained by both energy and angular momentum conservation. Vibrational deactivation from 6^1 has no energy constraint to overcome, and this is the reason that our ΔJ and ΔK distributions are exponential-like in form. Exponential-like distributions have been observed in pure rotational transfer of atom−diatomic collisions for many years.[40] It is not unreasonable for our system to exhibit similar behavior.

An interesting observation in this experiment is the near-uniformity of the 6_1^0 rotational contours for a particular collision partner. It appears that similar 0^0 distributions are created, with little dependence on the initial distribution of rotational levels in 6^1. All three collision partners displayed this behavior. Our analysis in sections IIID and IIIE showed that RET is not responsible for this, and the distributions reflect the rotational changes that accompany VET. One possible explanation is that the initial population distributions produced within 6^1 were not different enough to see an effect. However, the initial distributions cover a range of $\bar{J}$ (from 4 to 15 for H_2 and CH_4), and given, for example, the small $\Delta\bar{J}$ for H_2 (see above), this explanation does not appear tenable. The similarity of final distributions observed does not arise simply because ΔJ is much larger than the range of initial *J* values accessed. A feature of the fits of eq 1 with H_2 and, to a lesser extent, D_2 is that different parameters are required to fit the observed contours. In other words, similar final distributions are arrived at by the requirement that the parameters that govern the changes in rotational state depend on the initial *J* values. There is important information concerning the transfer dynamics here, and a more sophisticated approach is required to elucidate the mechanism responsible for the similarity of final state distributions. McCaffery has recently extended his angular momentum model to polyatomic transfer, and the data presented here offer a means to test this model.[11] Such an analysis will be undertaken and presented in a future publication.

V. Conclusions

A number of different rotational-level population distributions have been prepared in the 6^1 level of $^1B_{2u}$ benzene, and the resulting rotational distributions in 0^0 have been followed as collisions with H_2, D_2, or CH_4 transfer population to it. Care

has been taken to demonstrate that rotational-energy transfer within 6^1 and 0^0 does not obscure the rotational changes accompanying the vibrational change. The final rotational distributions in 0^0 showed little dependence on the initial 6^1 distribution with any of the collision partners.

The observed rotational contours were fit reasonably well by a thermal distribution. Fits to the observed contours using a momentum gap model showed that the probability for rotational transfer drops with increasing $|\Delta J|$ to a value of 1/e at $|\Delta J| = 4-6$ for H_2, $7-10$ for D_2, and 10 for CH_4. The $|\Delta K|$ changes are much larger for CH_4 than for H_2 and D_2, and it is likely that for a particular value of J the K states in 0^0 are populated fairly uniformly. A possible reason for the relaxed ΔK restriction with CH_4 may be that a broader range of collision geometries leads to vibrational-energy transfer. The distributions for D_2 are broader than those for H_2, illustrating that the reduced mass and rotational-level spacings play a role in determining the rotational changes occurring.

Acknowledgment. This work was undertaken with the financial support of the Australian Research Council and Flinders University. We are grateful to the technical support provided by the staff of the School of Chemistry, Physics and Earth Sciences Engineering and Electronic Workshops.

References and Notes

(1) Parmenter, C. S.; Tang, K. Y. *Chem. Phys.* **1978**, *27*, 127.
(2) Rice, S. A. *J. Phys. Chem.* **1986**, *90*, 3063.
(3) Krajnovich, D. J.; Parmenter, C. S.; Catlett, D. L. Jr. *Chem. Rev.* **1987**, *87*, 237.
(4) Flynn, G. W.; Parmenter, C. S.; Wodtke, A. M. *J. Phys. Chem.* **1996**, *100*, 12817.
(5) Waclawik, E. R.; Lawrance, W. D. *J. Chem. Phys.* **1998**, *109*, 5921.
(6) McCaffery, A. J.; Marsh, R. J. *Phys. Chem. Commun.* **2001**, *24*, 1.
(7) McCaffery, A. J.; Marsh, R. J. *J. Phys. Chem. A* **2000**, *104*, 10442.
(8) Marsh, R. J.; McCaffery, A. J. *Chem. Phys. Lett.* **2001**, *341*, 201.
(9) McCaffery, A. J.; Marsh, R. J. *J. Chem. Phys.* **2002**, *117*, 9275.
(10) Truhins, K.; Marsh, R. J., McCaffery, A. J.; Whiteley, T. W. J. *J. Chem. Phys.* **2000**, *112*, 5281.
(11) McCaffery, A. J. Private communication.
(12) Yardley, J. T. *Introduction to Molecular Energy Transfer*; Academic Press: New York, 1980.
(13) Gilbert, B. D.; Parmenter, C. S.; Krajnovich, D. J. *J. Chem. Phys.* **1994**, *101*, 7440.
(14) Waclawik, E. R.; Lawrance, W. D. *J. Chem. Phys.* **1995**, *102*, 2780.
(15) Riedle, E.; Knittel, T.; Weber, T.; Neusser, H. J. *J. Chem. Phys.* **1989**, *91*, 4555.
(16) Stephenson, T. A.; Radloff, P. L.; Rice, S. A. *J. Chem. Phys.* **1984**, *81*, 1060. Stephenson, T. A.; Rice, S. A. *J. Chem. Phys.* **1984**, *81*, 1073.
(17) Borg, R. A. J.; Waclawik, E. R.; Lawrance, W. D. *Chem. Phys. Lett.* **1992**, *199*, 320.
(18) de la Cruz, A.; Ortiz, M.; Campos, J. *Chem. Phys. Lett.* **1994**, *226*, 532.
(19) Waclawik, E. R.; Lawrance, W. D.; Borg, R. A. J. *J. Phys. Chem.* **1993**, *97*, 5298.
(20) Waclawik, E. R.; Mudjijono; Borg, R. A. J.; Lawrance, W. D. *Chem. Phys. Lett.* **1994**, *218*, 320.
(21) Waclawik, E. R.; Borg, R. A. J.; Mudjijono; Gascooke, J. R.; Hickman, C. G.; Lawrance, W. D. *Chem. Phys. Lett.* **1996**, *251*, 95.
(22) Jouvet, C. J.; Sulkes, M.; Rice, S. A. *Chem. Phys. Lett.* **1981**, *84*, 241.
(23) Miller, D. R. In *Atomic and Molecular Beam Methods*; Scoles, G., Ed.; Oxford University Press: Oxford, England, 1988; Vol. 1.
(24) Knight, A. E. W.; Parmenter, C. S.; Schuyler, M. W. *J. Am. Chem. Soc.* **1975**, *97*, 1993.
(25) Knight, A. E. W.; Parmenter, C. S.; Schuyler, M. W. *J. Am. Chem. Soc.* **1975**, *97*, 2005.
(26) Nicholson, J. A.; Lawrance, W. D.; Fischer, G. *Chem. Phys.* **1995**, *196*, 327.
(27) Herzberg, G. *Molecular Structure and Molecular Spectra III: Electronic Spectra and Electronic Structure of Polyatomic Molecules*; Van Nostrand Reinhold: Toronto, 1966.
(28) Callomon, J. H.; Dunn, T. M.; Mills, I. M. *Philos. Trans. R. Soc. London, Ser. A* **1966**, *259*, 499.
(29) Pliva, J.; Pine, A. S. *J. Mol. Spectrosc.* **1982**, *93*, 209.
(30) Herzberg, G. *Molecular Structure and Molecular Spectra I: Spectra of Diatomic Molecules*; Van Nostrand Reinhold: Toronto, 1950.
(31) Chapman, W. B.; Schiffman, A.; Hutson J. M.; Nesbitt, D. J. *J. Chem. Phys.* **1996**, *105*, 3497.
(32) Mills, I. M. *Mol. Phys.* **1964**, *7*, 549.
(33) Whetton, N. T.; Lawrance, W. D. *J. Phys. Chem.* **1992**, *96*, 3717.
(34) Coveleskie, R. A.; Parmenter, C. S. *J. Chem. Phys.* **1978**, *69*, 1044.
(35) Clegg, S. M.; Burrill, A. B.; Parmenter, C. S. *J. Phys. Chem. A* **1998**, *102*, 8477.
(36) Clegg, S. M.; Parmenter, C. S. *J. Phys. Chem. A* **2000**, *104*, 10265.
(37) Steinfeld, J. I.; Ruttenberg, P.; Millot, G.; Fanjoux, G.; Lavorel, B. *J. Phys. Chem.* **1991**, *95*, 9638.
(38) Weston, R. E., Jr.; Flynn, G. W. *Annu. Rev. Phys. Chem.* **1992**, *43*, 559.
(39) Clare, S.; Marks, A. J.; McCaffery, A. J. *J. Chem. Phys.* **1999**, *111*, 9287.
(40) Stewart, B.; Magill, P. D.; Pritchard, D. E. *J. Phys. Chem. A.* **2000**, *104*, 10565.